

PCCP

Accepted Manuscript



This is an *Accepted Manuscript*, which has been through the Royal Society of Chemistry peer review process and has been accepted for publication.

Accepted Manuscripts are published online shortly after acceptance, before technical editing, formatting and proof reading. Using this free service, authors can make their results available to the community, in citable form, before we publish the edited article. We will replace this *Accepted Manuscript* with the edited and formatted *Advance Article* as soon as it is available.

You can find more information about *Accepted Manuscripts* in the [Information for Authors](#).

Please note that technical editing may introduce minor changes to the text and/or graphics, which may alter content. The journal's standard [Terms & Conditions](#) and the [Ethical guidelines](#) still apply. In no event shall the Royal Society of Chemistry be held responsible for any errors or omissions in this *Accepted Manuscript* or any consequences arising from the use of any information it contains.

***In situ* synthesis of Ni(OH)₂ nanobelts modified electroactive poly(vinylidene fluoride) thin films: Remarkable improvement in dielectric properties**

Pradip Thakur^{1,2}, Arpan Kool¹, Biswajoy Bagchi¹⁺, Nur Amin Hoque,¹ Sukhen Das^{1++*}, Papiya Nandy¹

¹Department of Physics, Jadavpur University, Kolkata- 700032, India

²Department of Physics, Netaji Nagar College for Women, Kolkata-700092, India

⁺Present address: Fuel Cell and Battery Division, Central Glass and Ceramic Research Institute, Kolkata- 700032, India.

⁺⁺ Present address: Department of Physics, IEST, Howrah, West Bengal - 711103, India.

*Corresponding author. Email address: sdasphysics@gmail.com, Mobile: +919433091337

ABSTRACT: A facile and low cost synthesis of Ni(OH)₂ nanobelts (NBs) modified electroactive poly(vinylidene fluoride) (PVDF) thin films with excellent dielectric properties has been prepared via *in situ* formation of Ni(OH)₂ NBs in PVDF matrix. Formation and morphology of the NBs are confirmed by UV-Visible spectroscopy and Field emission scanning electron microscopy respectively. A remarkable improvement in electroactive β phase nucleation (~82%) and dielectric constant ($\epsilon \sim 3.1 \times 10^6$ at 20 Hz) have been observed in the nanocomposites (NCs). The interface between the NBs and the polymer matrix plays a crucial role in the enhancement of electroactive β phase and the dielectric properties of the thin films. Strong interaction via hydrogen bond between Ni(OH)₂ NBs and PVDF matrix is the main reason for enhancement β phase crystallization and improved dielectric properties. The NC thin films can be utilized for potential applications as high energy storage devices

like supercapacitors, solid electrolyte batteries, self-charging power cells, piezoelectric nanogenerator, thin film transistors and sensors.

KEYWORDS: *In situ*, Ni(OH)₂, nanobelt, PVDF, interfacial polarization, dielectric constant

1. INTRODUCTION

Electroactive polymer nanocomposites (NCs) with colossal dielectric properties have drawn tremendous interest due to their diverse applications including high energy density arrays of capacitors, light switches or displays, piezoelectric or pyroelectric sensors, thin film transistors, non-volatile memories and most recently in biomedical and electronic fields.¹⁻⁷

Studies on spontaneously polarized or ferroelectric polymers are increasingly gaining importance due to their excellent dielectric, piezoelectric, pyroelectric, ferroelectric and electro-optic properties. The basic key element of electrical and electromechanical responses of these electroactive polymers is the storage and movement of electrical charges in the polymer matrix. Hence, the development of electroactive polymer NCs with high electric energy densities, which are dependent on dielectric constant and applied electric field strength have gained tremendous interest worldwide.¹⁻⁶

Poly(vinylidene fluoride) (PVDF) is a well known electroactive semicrystalline polymer with five different crystalline phases α , β , γ , δ and ϵ . Among these nonpolar α phase with TGTG' (T-trans, G-gauche⁺, G'-gauche) dihedral conformation is thermodynamically more stable at room temperature and pressure than the other phases. Polar or electroactive β phase with TTTT conformation exhibits highest piezoelectric, pyroelectric and ferroelectric property than other phases. On the other hand, polar γ phase with TTTGTTG' conformation exhibits moderate piezoelectricity.⁷⁻⁹ Thus, improving the electroactive β phase nucleation in PVDF may lead to diverse application of the polymer.

Although many research works have been reported to develop the electroactive β phase crystallization in PVDF and consequently to achieve improved dielectric properties in polymer NCs by introducing different fillers like clays,⁹⁻¹² ceramic filler,¹³ metal nanoparticles (NPs),^{14,15} ferrites,^{16,17} hydrated inorganic salts,¹⁸ carbon nanotubes,^{19,20} graphene,²¹ metal oxide NPs²²⁻²⁴ etc. However, very few have reported on the interfacial effects of transition metal hydroxide NPs in PVDF matrix on the electroactive β phase nucleation and the dielectric performance of the NCs. Dielectric properties and electroactive β phase of PVDF based NCs filled with surface hydroxylated BaTiO₃ (h-BT) and crude BaTiO₃ (c-BT) NPs have been reported by Zhou et al.²⁵ The h-BT/PVDF NCs have showed lower tangent loss and higher dielectric strength as well as more electroactive β phase nucleation than the c-BT/PVDF NCs. Later, improvement in β phase nucleation in PVDF has been observed in the surface hydroxylated nickel NPs-PVDF composite by Mandal et al.²⁶ In our present work, we report a simple and effective approach to develop electroactive polymer NC thin films with significantly high dielectric constant via *in situ* synthesis of Ni(OH)₂ nanobelts (NBs) in PVDF matrix. The effect of the interfaces between the Ni(OH)₂ NBs and the polymer matrix on the electroactive β phase crystallization and dielectric properties have been thoroughly studied.

2. EXPERIMENTAL

2.1. Materials

The materials used in the synthesis of NC thin films are poly(vinylidene fluoride) (Aldrich, Germany. M_w : 275000 (hpc), M_n : 107000), nickel chloride hexahydrate (NiCl₂, 6H₂O) (Merck, India), sodium borohydrate (NaBH₄) (Merck, India), dimethyl sulfoxide (DMSO) (Merck, India).

2.2. *In situ* synthesis of Ni(OH)₂ NBs modified PVDF thin films

Initially, PVDF was dissolved in DMSO (3.33 mass %) at 60°C under vigorous stirring. Then, different molar concentrations (0.01-0.30 (M)) of NiCl₂ · 6H₂O salt was dissolved in the previously prepared PVDF-DMSO solution under constant magnetic stirring followed by slow addition of appropriate amount of 1 (M) NaBH₄ solution in DMSO under ambient condition. The addition of NaBH₄ reduced the metal to its corresponding hydroxide NPs in air. The colour changes from homogeneous green to blackish finally pale green indicated the formation of Ni(OH)₂ NPs in the PVDF matrix. The thin films were obtained by casting the Ni(OH)₂ NBs loaded PVDF solutions in clean Petri dishes and evaporating the solvent in a dust free oven at 80 °C for 24 hours. Pure PVDF film was also prepared under same condition. All the samples were dried in vacuum for 24 hours and stored in vacuum desiccator for further studies. The thickness of as-prepared films were in the range of 70-80 μm. The sample designations have been represented in Table 1.

Table 1 Sample Designation.

Name of the Samples	Amount of PVDF taken in 15 ml DMSO (mg)	Amount of Ni salt added (M)	Corresponding percentage of the NBs (volume %)
PNi 0.01	500	0.01	1.2
PNi 0.05		0.05	5.7
PNi 0.10		0.10	10.7
PNi 0.15		0.15	15.5
PNi 0.20		0.20	19.4
PNi 0.25		0.25	23.1
PNi 0.30		0.30	26.5
PVDF	500	0	0

2.3. Characterizations

The formation of Ni(OH)₂ NBs in NCs thin films was investigated using UV-Visible spectrophotometer (UV-3101PC, Shimadzu) in the wavelength range 300-800 nm. The morphology and microstructures of the fractured surfaces of the NC thin films were observed using Field emission scanning electron microscope (FESEM) ((INSPECT F50, Netherlands).

Electroactive β phase nucleation in the films were investigated using X-ray diffractometer (Model-D8, Bruker AXS Inc., Madison, WI) with scan speed of 0.5 s/step and an operating voltage of 40 kV with 2θ range from 15° to 60° using Cu-K α radiation. Then the samples were further characterized using Fourier transform infrared spectroscopy (FTIR-8400S, Shimadzu) to determine the effect of NBs on phase crystallization. The absorbance data of the films were noted in the wavenumber range from 400 cm⁻¹ to 1100 cm⁻¹ with a resolution of 4 cm⁻¹. 50 scans were carried out for each sample. The fraction of β -phase ($F(\beta)$) in the films were calculated from IR spectra using Lambert-Beer law as follows,

$$F(\beta) = \frac{A_{\beta}}{\left(\frac{K_{\beta}}{K_{\alpha}}\right)A_{\alpha} + A_{\beta}} \quad (1)$$

Where, A_{α} and A_{β} are the absorbance at 764 cm⁻¹ and 840 cm⁻¹, respectively and K_{β} (7.7×10^4 cm² mol⁻¹) and K_{α} (6.1×10^4 cm² mol⁻¹) are the absorption coefficients at the respective wavenumber.^{9, 16, 24}

The Micro-Raman spectra of the samples were investigated using a Jobin Labram HR spectrometer (Horiba Jobin Yvon Tech., France). A He-Ne laser of wavelength 785 nm was

used to excite the samples and the data were recorded in the wavenumber range from 400 cm⁻¹ to 1000 cm⁻¹.

The crystallization and melting behaviour of the pure PVDF and NBs modified PVDF thin films were analysed using a Differential scanning calorimeter (DSC-60, Shimadzu (Asia Pacific) Pte. Ltd., Singapore) under N₂ gas atmosphere. All the samples were heated from 80°C to 200°C at a heating rate of 5°C/min. The degree of crystallinity (X_c) of the films was calculated from DSC thermographs using the following equation:

$$X_c = \Delta H_m / \Delta H_{100\%} \quad (2)$$

Where, ΔH_m is the melting enthalpy of the films and $\Delta H_{100\%}$ is the melting enthalpy of 100% crystalline PVDF with value 104.6 J/gm.^{9, 24}

The capacitance (C) and tangent loss ($\tan\delta$) were studied using digital LCR meter (Agilent, E4980A) at 1 V signal for the frequency range from 20 Hz to 1 MHz in a sample holder contained circular Ag electrodes at ambient condition. The dielectric constant (ϵ) and the ac conductivity (σ_{ac}) of the samples were calculated using following equations respectively,

$$\epsilon = C.d / \epsilon_0 A \quad (3) \quad \text{and} \quad \sigma_{ac} = 2\pi f \epsilon_0 \epsilon \tan\delta \quad (4)$$

where, d and A are the thickness and area of the samples respectively and f is the frequency in Hz applied across the films and ϵ_0 is permittivity of free space with value 8.854×10^{-12} F.m⁻¹.

^{9, 24}

3. RESULTS AND DISCUSSIONS

3.1. UV-Visible spectroscopy

The UV-Visible absorbance of pure PVDF and the Ni(OH)₂ NBs modified PVDF thin films (PNi 0.01, PNi 0.05, PNi 0.10, PNi 0.15, PNi 0.20, PNi 0.25 and PNi 0.30) are shown in Figure 1. For pure PVDF film no characteristic absorption peak was observed.

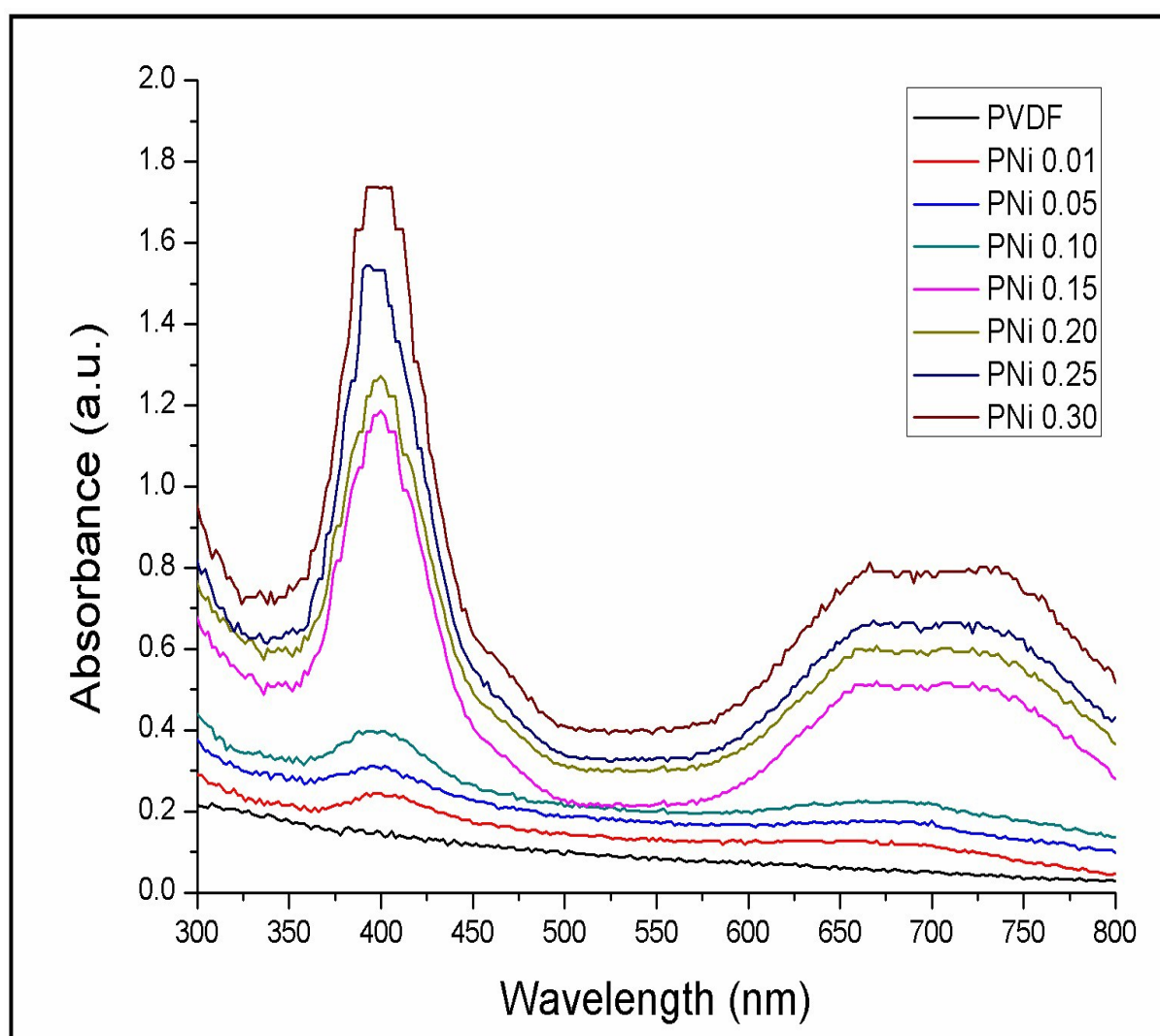


Figure 1: UV-Visible absorption spectra of pure PVDF and Ni(OH)₂ NBs modified PVDF thin films.

But for Ni(OH)₂ NBs modified PVDF thin films two wide absorption peaks centred at 375-440 nm (~3.1 eV) and 650-750 nm (~1.77 eV) were observed which confirms the formation of Ni(OH)₂ NBs in PVDF matrix. It was also observed that the absorption intensity of two absorptions peaks is increased with the Ni(OH)₂ content confirming the completion of the reaction between salt and NaBH₄ to Ni(OH)₂. The two absorption peaks are due to the transitions of Ni²⁺ in oxygen octahedral sites from the ground state ³A_{2g} to ³T_{1g}(P) and ³T_{1g}(F) states.²⁷⁻²⁹

3.2. Morphology and Microstructure of the Ni(OH)₂ NBs modified PVDF thin films

The morphology and microstructures of pure PVDF and Ni(OH)₂ NBs-PVDF thin films as well as formation of NBs were investigated using field emission scanning electron microscopy (FESEM). Figure 2 and 3 show the FESEM images of the samples. Formation of well define uniformly distributed belt like Ni(OH)₂ nanostructures (about 200 nm width) have been observed up to 23.1 volume% doped films (PNi 0.01, PNi 0.05, PNi 0.10, PNi 0.15, PNi 0.20 and PNi 0.25) but for PNi 0.30 sample the Ni(OH)₂ is agglomerated in the PVDF matrix.

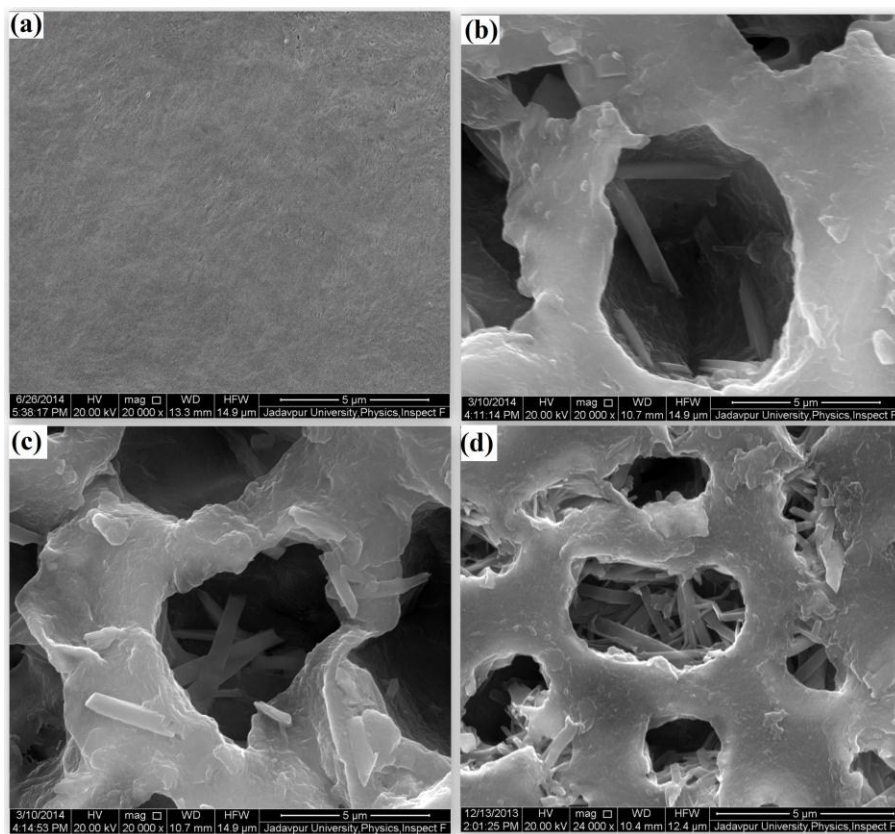


Figure 2: FESEM images of (a) pure PVDF and the fractured surface of (b) PNi 0.01, (c) PNi 0.05 and (d) PNi 0.10 samples.

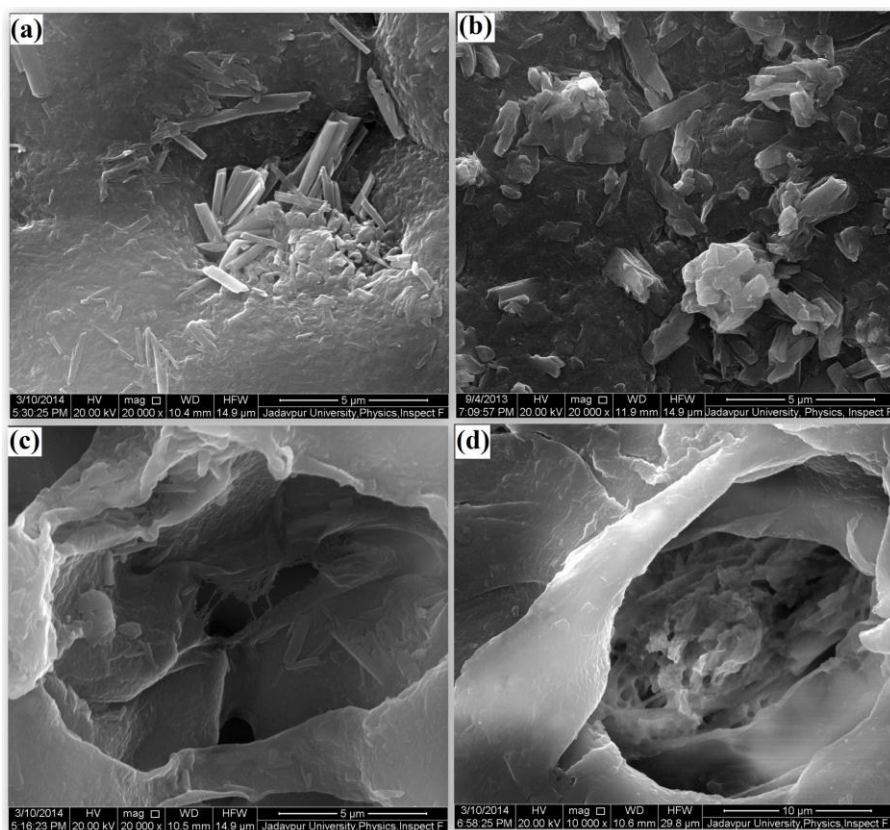


Figure 3: FESEM images of the fractured surface of (a) PNi 0.15, (b) PNi 0.20, (c) PNi 0.25 and (d) PNi 0.30 samples.

3.3. Formation of electroactive β phase in PVDF

3.3.1. X-ray diffraction analysis

The crystal structures of pure PVDF and the $\text{Ni}(\text{OH})_2$ NBs modified PVDF thin films were studied using X-ray diffractometer. Figure 4a shows the X-ray diffraction (XRD) patterns of pure PVDF and $\text{Ni}(\text{OH})_2/\text{PVDF}$ films. The peaks corresponding to $\text{Ni}(\text{OH})_2$ NBs and any other possible impurity phases were not observed in any of these XRD patterns. Thus XRD pattern also confirmed formation of non-crystalline or amorphous $\text{Ni}(\text{OH})_2$ NBs and uniform distribution of the NBs in PVDF matrix. The diffraction pattern of pure PVDF shows peaks at 2θ values of 17.4° (100), 18.0° (020), 19.7° (021) and 26.3° ((201), (310)) corresponding to α phase and 38.5° (211) for γ phase. But in the $\text{Ni}(\text{OH})_2/\text{PVDF}$ films, all peaks corresponding

to α or γ phases disappeared indicating phase transformation. Only two characteristic peaks of electroactive β phase appear at 20.5° ((110), (200)) and 36.4° ((020), (101)) confirming β phase nucleation in the nanocomposite samples.^{7,9}

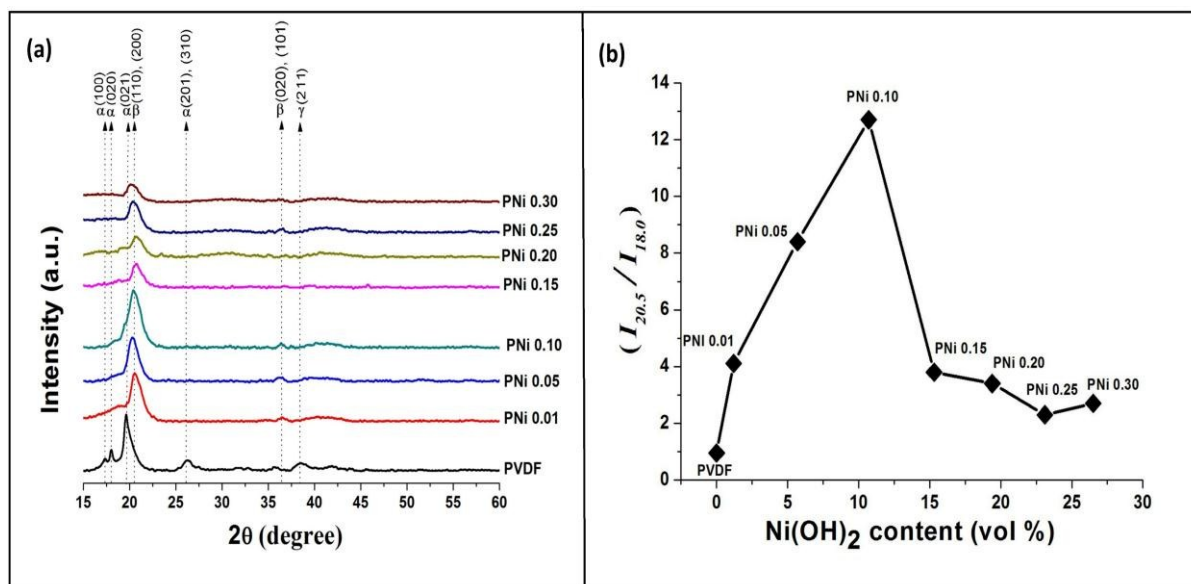


Figure 4: (a) XRD patterns of pure PVDF and Ni(OH)_2 NBs modified PVDF thin films and (b) Ratio of $I_{20.5}$ and $I_{18.0}$ of the thin films.

However on a closer observation of the XRD patterns show that the intensity and sharpness of the main peak of β -phase ($2\theta = 20.5^\circ$) have been increased up to 10.7 volume % loaded samples and then decreased for higher NBs concentrations. The ratio of the intensity of the peak at 20.5° and 18.0° ($I_{20.5} / I_{18.0}$) yields an measure of α and β phase content in samples.²⁶ In pure PVDF, the ratio is found to be 0.95, which increases with Ni(OH)_2 NBs content and attains maximum value 12.7 for PNi 0.10 (Figure 4b). Thus, XRD results suggest that the electroactive β phase crystallization in PVDF is significantly improved due to nucleating action of the Ni(OH)_2 NBs.

3.3.2. Fourier transform infrared spectroscopy

Fourier transform infrared (FTIR) spectroscopy is one of the finest techniques for determining α , β , and γ phases of PVDF. FTIR study have been performed to investigate different crystalline polymorphs present in pure PVDF and Ni(OH)₂/PVDF thin films which is shown in Figure 5. The FTIR spectrum of pure PVDF exhibits absorbance bands at 489 cm⁻¹ (CF₂ wagging) 533 cm⁻¹ (CF₂ bending), 615 and 764 cm⁻¹ (CF₂ bending and skeletal bending), 796 and 975 cm⁻¹ (CH₂ rocking) corresponding to α -phase and tiny absorbance band at 840 cm⁻¹ (CH₂ rocking, CF₂ stretching and skeletal C-C stretching) which is due to β phase (Figure 5a).

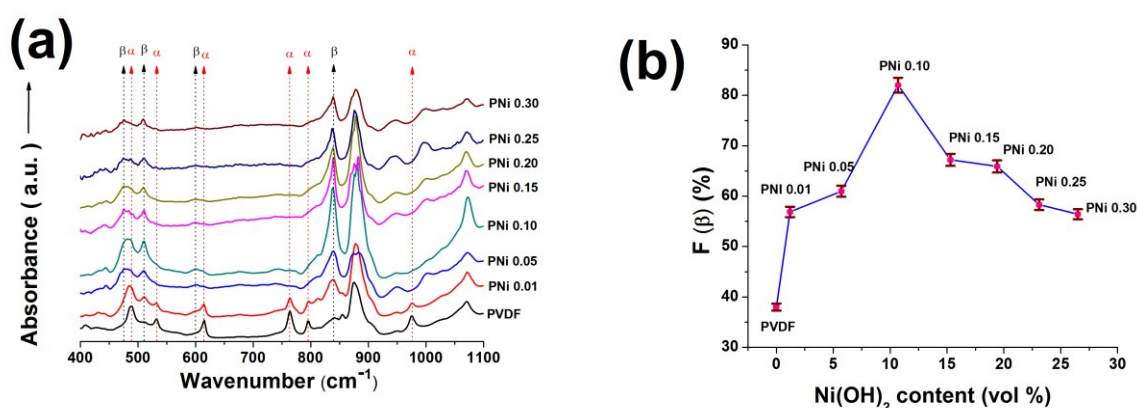


Figure 5: (a) FTIR spectra of pure PVDF and Ni(OH)₂ NBs modified PVDF thin films and (b) $F(\beta)$ of the thin films. Error bars represent the standard deviation of the experiment conducted in triplicate and were assessed by one way ANOVA using graph pad Instat version 5.0 software.

But, for Ni(OH)₂ NBs loaded PVDF films all characteristic absorbance bands corresponding to α phase are almost absent. Only the band at 615 cm⁻¹ is still present for sample PNi 0.01, PNi 0.05 and PNi 0.10 but for other samples the absorbance bands corresponding to α phase are totally diminished. The characteristic absorbance bands due to electroactive β phase at 476 cm⁻¹ (CF₂ deformation) 510 cm⁻¹ (CF₂ stretching), 600 cm⁻¹ (CF₂ wag) and 840 cm⁻¹ (CH₂ rocking, CF₂ stretching and skeletal C-C stretching) are appeared prominently for all NBs modified polymer samples.^{7, 9, 30} The intensity of β -PVDF characteristic bands is

significantly increased up to 10.7 volume% Ni(OH)₂ NB loaded PVDF films and then decreases at higher NB concentrations. The decrease in β -PVDF characteristic bands may be attributed to the confinement of the movements of polymer chains to longer TTTT conformation due to high doping of the NBs.

The fraction of electroactive β phase content ($F(\beta)$) in pure PVDF and Ni(OH)₂ NBs loaded PVDF thin films have been calculated from FTIR spectra using equation 1. Variation of $F(\beta)$ (%) with the NBs content (volume%) is graphically presented in Figure 5b. For pure PVDF $F(\beta)$ is found to be 38 % which increases with Ni(OH)₂ NBs content. The $F(\beta)$ is attained a maximum value of 82 % at 10.7 volume% loading of Ni(OH)₂ NBs in PVDF matrix. Thus, it is also confirmed from FTIR spectroscopy that the electroactive β phase stabilization and nucleation is accelerated by the Ni(OH)₂ NBs.

3.3.3. Raman spectroscopy

Figure 6 represents the micro-Raman spectra of the samples which also confirmed the formation of electroactive β phase in the Ni(OH)₂ NBs modified PVDF thin films.

In pure PVDF film, only one Raman band at 796 cm⁻¹ (CH₂ rocking) corresponding to nonpolar α phase is observed. But for Ni(OH)₂/PVDF thin films the Raman intensity of the band 796 cm⁻¹ is decreased. Four new Raman bands at 510 cm⁻¹ (CF₂ stretching) (PNi 0.05 and PNi 0.10) and 840 cm⁻¹ (CH₂ rocking, CF₂ stretching and skeletal C-C stretching) corresponding to electroactive β phase, 812 cm⁻¹ (CH₂ out-of plane wag) corresponding to polar γ phase have been appeared.^{9, 30} Once again, the Raman intensity of the main β -PVDF bands at 510 cm⁻¹ and 840 cm⁻¹ attained maximum for PNi 0.10 sample which is consistent with XRD and FTIR data.

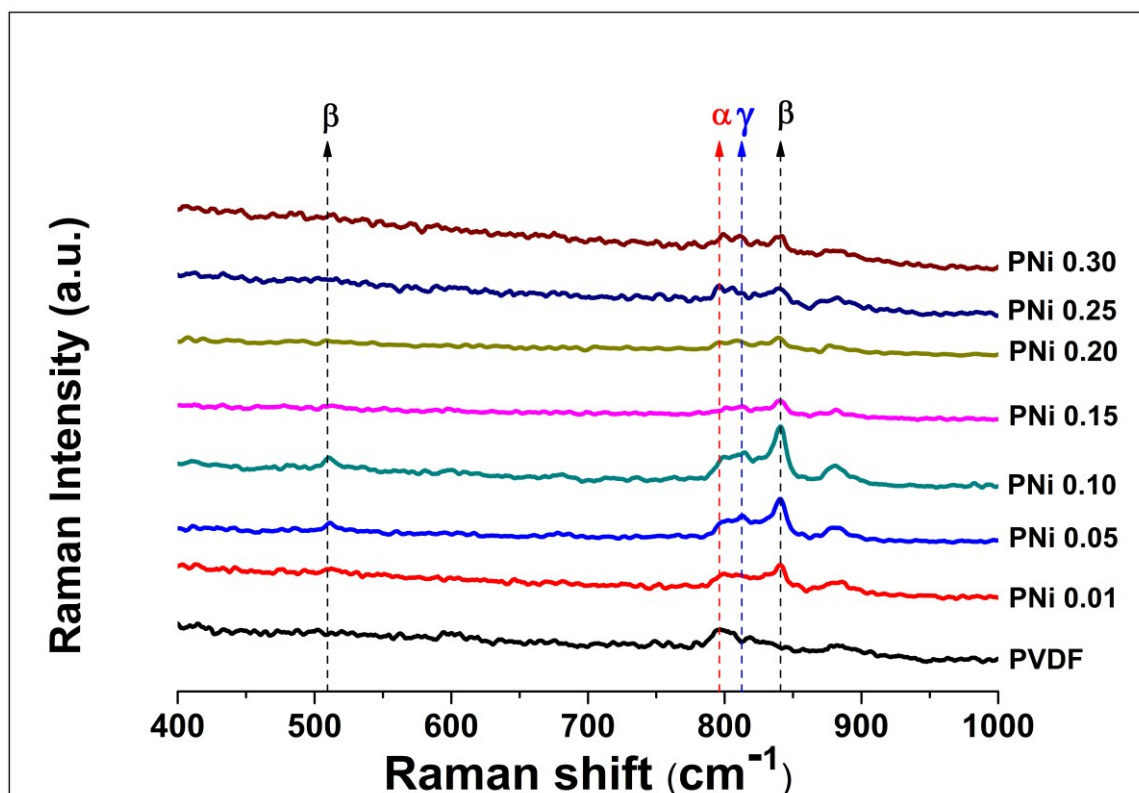


Figure 6: Micro-Raman spectra of pure PVDF and Ni(OH)₂ NBs modified PVDF thin films.

3.3.4. Differential scanning calorimetry

Differential scanning calorimetry (DSC) was also used to complement XRD, FTIR and Raman spectroscopy data for the identification of different crystalline phases of PVDF. Figure 7 shows the DSC thermographs of the samples. A strong melting peak at 163.62°C suggested α phase crystallization and a tiny side peak at 166.3°C refers to some presence of electroactive β phase content in pure PVDF thermograph. However, the melting temperature (T_m) of the NBs loaded films was found to increase by almost 5°C. This is suggested due to more β -phase nucleation in the Ni(OH)₂ NBs modified PVDF films than the pure PVDF film which is consistent with XRD, FTIR and Raman spectroscopy results.^{9, 12, 20}

DSC thermographs give the information about the enthalpies of fusion or melting enthalpies as well as the degree of crystallinity of the samples. The melting enthalpies (ΔH_m (J/g)) of pure PVDF and the Ni(OH)₂ NBs modified PVDF films are evaluated from the DSC thermographs. Therefore, the degree of crystallinity (X_c) of the thin films are calculated using equation 2. An increase in melting enthalpies is observed up to 10.7 volume% Ni(OH)₂ NBs loaded samples compared to pure PVDF and then decreases for higher loading of the NBs in PVDF matrix implying an increase in X_c values also (Figure 7b and c).

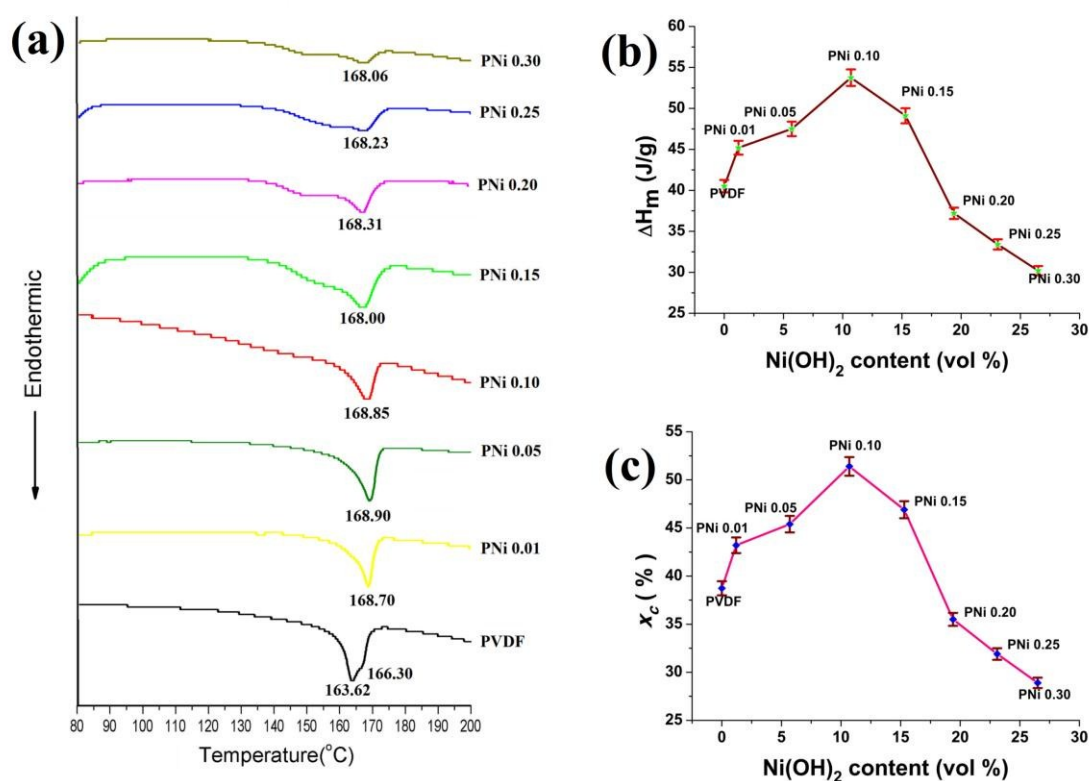


Figure 7: (a) DSC thermographs of pure PVDF and Ni(OH)₂ NBs modified PVDF thin films and Evaluation of (b) enthalpy of fusion and (c) degree of crystallinity of pure PVDF and Ni(OH)₂ NBs modified PVDF thin films with increasing NPs content from DSC thermographs. Error bars represent the standard deviation of the experiment conducted in triplicate and were assessed by one way ANOVA using graph pad Instat version 5.0 software.

The X_c values increase with the NBs content and achieve maximum about 53.75% for 10.7 volume% loading (PNi 0.10) (Figure 7c). Increase in crystallinity than pure PVDF for lower loading of the Ni(OH)₂ NBs (up to 10.7 volume%) is due to the nucleating action of the NBs.^{9, 24} Higher doping of the NBs in PVDF leads to confinement of the movements of the polymer chains and deceleration of the nucleating or catalytic action of the NBs as the number of nucleation points grows so much that the β spherulites i.e. grains cannot be formed resulting decrease in X_c values.^{9, 24, 31}

3.4. Mechanism of electroactive β phase crystallization

Though the nucleation of electroactive β phase in the samples is observed by XRD, FTIR, Raman spectroscopy and DSC data and the interfacial interaction has been observed by FESEM micrographs. It is necessary to investigate the possible interaction between the Ni(OH)₂ NBs and the polymer which promotes the electroactive β phase crystallization in the NCs. Our previous work on clay mineral-PVDF and Fe₂O₃ or Co₃O₄ NPs-PVDF thin films suggest that the strong interaction between the positive CH₂ dipoles of the polymer chain and the negatively charged surfaces of the clay minerals or the NPs leads to stabilized longer TTTT conformation on the clay mineral surfaces.^{9, 24}

In present study, the formation of electroactive β -phase may be discussed in terms of hydrogen bonds development in the NC films which leads stronger interaction between Ni(OH)₂ NBs and the PVDF matrix.^{25, 26} When the Ni(OH)₂ NBs are formed by *in situ* process in PVDF matrix, the hydrogen bonds are formed between the fluorine (F) atoms of PVDF and the -OH groups of the Ni(OH)₂ NBs. During the films formation at 80 °C, the surfaces of NBs act as substrates of β -phase crystallization. Thus, strong interaction between the F atoms of PVDF and the -OH groups Ni(OH)₂ NBs leads to the alignment of stabilized PVDF chains on the surfaces of NBs in longer all trans or TTTT conformation i.e.

electroactive β phase. Similar type of interactions between the fluorine (F) atoms of PVDF and the -OH groups via hydrogen bonds were reported in dielectric study of hydroxylated BaTiO₃- PVDF composites²⁵ and magneto-dielectric study of hydroxylated Ni-PVDF composites.²⁶

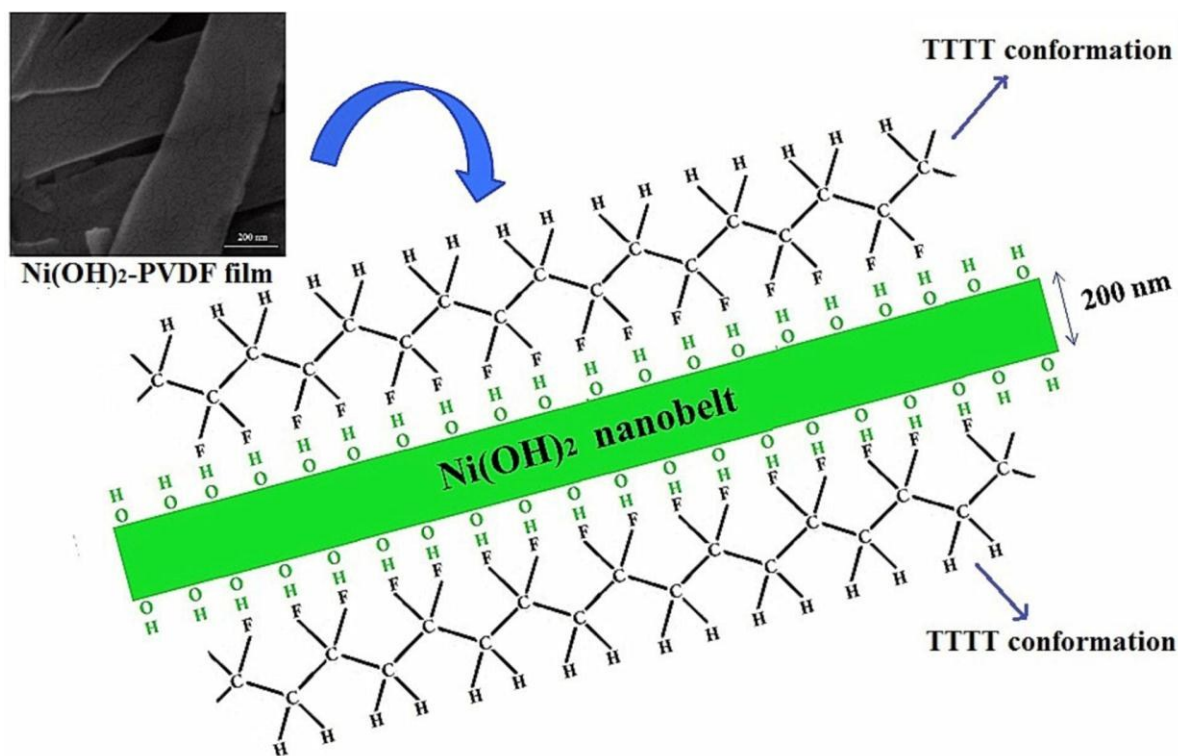


Figure 8: Schematic diagram of proposed β phase transformation mechanism.

The existence of small amount of TTTGTTTG' conformation i.e. γ phase (Figure 6) in some films is due to gauge effect developed due to easier local internal chain rotation. Figure 8 shows the schematic diagram of possible interaction mechanism between the NBs and PVDF chains during the formation of electroactive β -phase.

3.5. Dielectric properties of the thin films

3.5.1. Ni(OH)_2 content dependence of the dielectric properties

Figure 9 shows the variation of dielectric constant and tangent loss of the Ni(OH)₂ NB modified PVDF films as a function of NB content at 20 Hz, 10 KHz, 100 KHz and 1 MHz. Increase in dielectric constants with Ni(OH)₂ NBs loading have been observed up to 23.1 volume% loading of NBs and decreases for further loading. Tangent losses of Ni(OH)₂ NBs loaded PVDF films increase in a nonlinear fashion with NB content due to occurrence of different Debye like relaxations i.e. tangent loss peak at different frequency for different loading of the NBs. Closer observation shows that for higher frequencies (100 KHz and 1 MHz) the dielectric constants of the NCs have been increased almost linearly with Ni(OH)₂ NBs content up to 23.1 volume% loading of the NB, suggesting that the high frequency dielectric constant of the NCs are influenced by the dipolar polarization of Ni(OH)₂ NB itself.

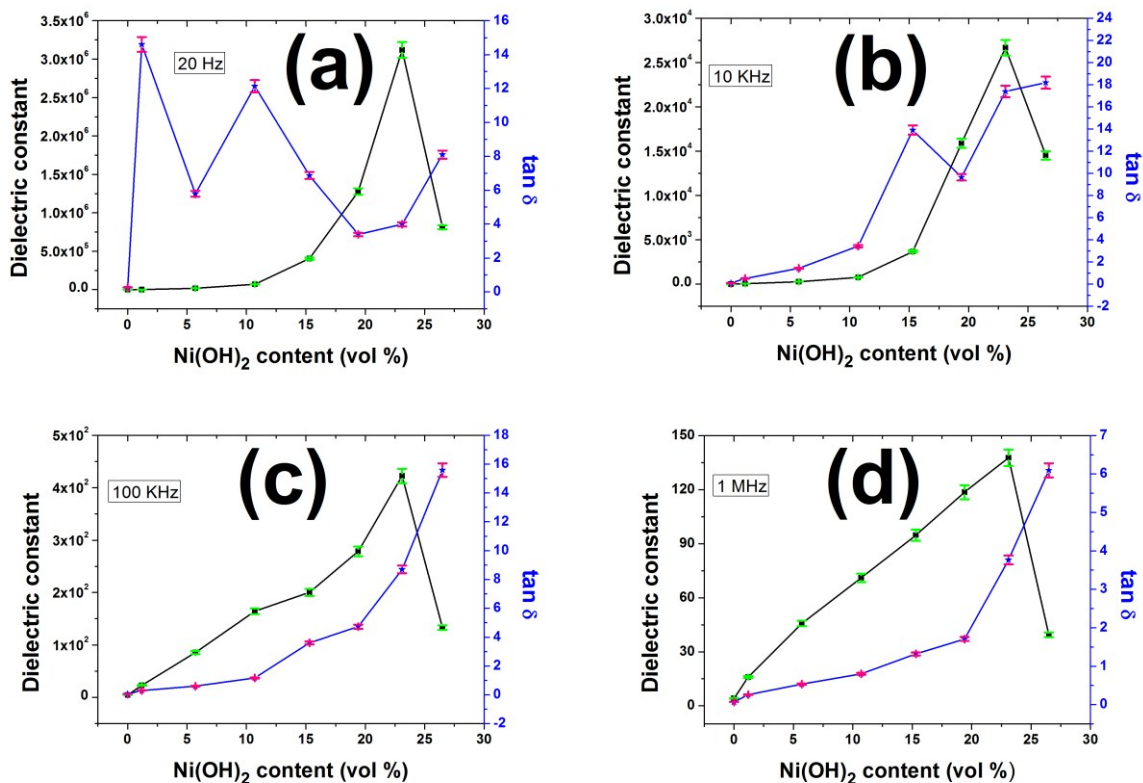


Figure 9: Ni(OH)₂ NBs content dependence of dielectric constants and tangent losses at (a) 20 Hz, (b) 10 KHz, (c) 100 KHz and (d) 1 MHz. Error bars represent the standard deviation of the experiment

conducted in triplicate and were assessed by one way ANOVA using graph pad Instat version 5.0 software.

At low frequencies (20 Hz and 10 KHz) dielectric constant improves linearly up to 10.7 volume% loading of the NBs but a dramatic improvement of dielectric constant in a nonlinear fashion has been observed for higher loading of the NBs up to 23.1 volume% which may be due to reaching the percolation threshold.

Figure 10 shows the dependence of ac conductivities of the samples on NBs loading concentrations at 20 Hz, 10 KHz, 100 KHz and 1 MHz. Like dielectric constant, a sharp increase in ac conductivity at 23.1 volume% loading Ni(OH)₂ NBs is also observed for lower frequencies (20 Hz and 10 KHz) and linear increment for higher frequencies (100 KHz and 1 MHz).

The tremendous improvement in dielectric constant at lower frequencies upon reaching percolation threshold is mainly from the interaction between polymer chain and NBs is because of two facts: firstly, due to the occurrence of the synergetic effect between the PVDF matrix and the Ni(OH)₂ NBs fillers, mainly at lower concentration of the NBs (23.1 volume%).²⁰ There are still no report about the dielectric constant of Ni(OH)₂ NPs. So, to verify the synergetic effect, we have prepared Ni(OH)₂ NPs under same condition and found the dielectric constant of Ni(OH)₂ to be about ~ 3500 at 20 Hz. It is to be noted that the dielectric constant (~3.1 x 10⁶ at 20 Hz) of the NC is larger than PVDF and Ni(OH)₂ alone. Secondly, due to the Maxwell-Wagner-Sillars (MWS) interfacial polarization effect which appears in heterogeneous medium consisting of phases with different dielectric constant and conductivity i.e. with different relaxation time due to accumulation of the charges at the interfaces of the two dielectric materials.^{9, 25, 32-36} Thus, due to difference in dielectric properties or difference in relaxation time the charge carriers are confined significantly at the

interfaces of the PVDF and Ni(OH)₂ NBs (Figure 8) resulting in strong MWS interfacial polarization and huge improvement of the dielectric constant of modified PVDF thin films. The effective interfacial areas between the NBs and polymer matrix i.e. the MWS interfacial polarization effect is also intensified greatly due to the formation of donor-acceptor complexes or the hydrogen bonds between the F atoms of PVDF chains and the -OH groups of the Ni(OH)₂ NB at Ni(OH)₂-PVDF interfaces.^{25, 37} The NBs are well separated from each other with no such effective interaction between them at low concentration. But, with increase in Ni(OH)₂ NB content, the interfacial area per unit volume increases while the inter particle distance decreases. This raises the average polarization linked with the NBs and coupling between neighboring grains of polymer resulting in colossal dielectric improvement of the thin films. Homogeneous distribution of the NBs in PVDF matrix up to 23.1 volume% loading (Figure 2 and 3) results in large interfacial area per unit volume of the NBs which significantly enhances the MWS interfacial polarization in the films.³⁵

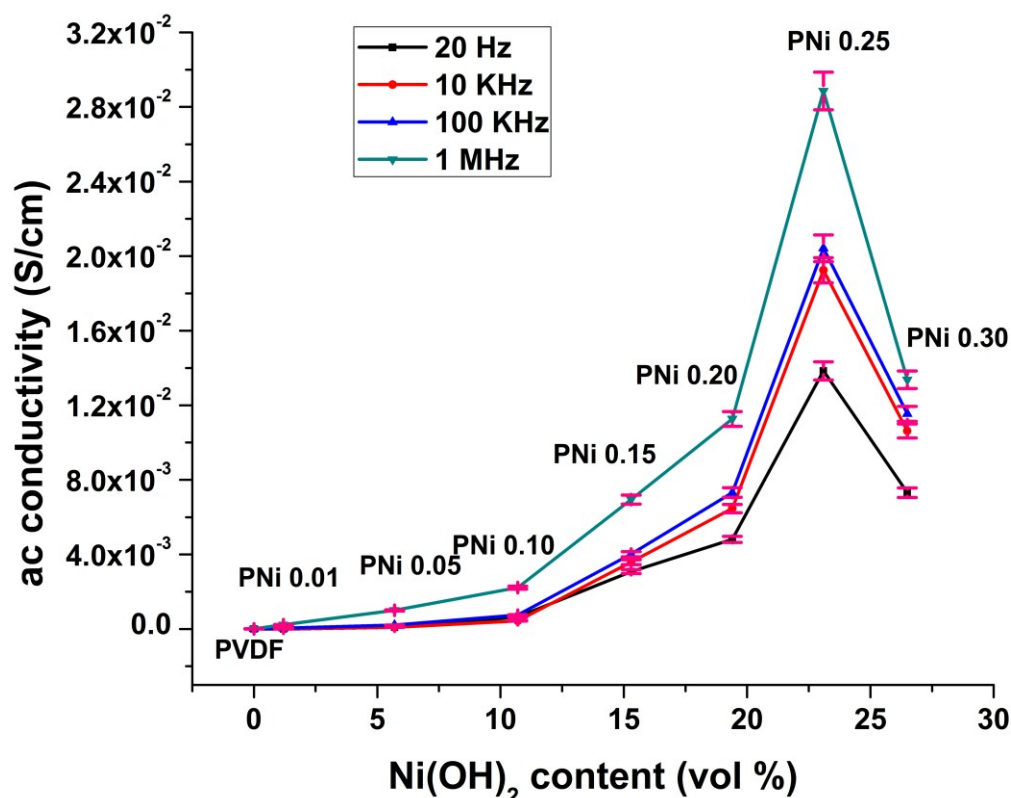


Figure 10: Ni(OH)₂ NBs content dependence of ac conductivities at 20 Hz, 10 KHz, 100 KHz and 1 MHz. Error bars represent the standard deviation of the experiment conducted in triplicate and were assessed by one way ANOVA using graph pad Instat version 5.0 software.

Further loading of the NBs reduces the interfacial area per unit volume as well as the dielectric constant and ac conductivity due to agglomeration of the NBs (Figure 3b).

3.5.2. Frequency dependence of the dielectric properties

Figure 11 shows the frequency dependence of the dielectric constant and tangent loss of the Ni(OH)₂ NBs modified PVDF thin films at room temperature and atmospheric pressure. Noticeable steplike decrease in dielectric constant towards high frequencies (Figure 11a) associated with tangent loss peaks at different frequencies (Figure 11b) have been observed. This step like reduction in dielectric constant with frequency is readily explained by MWS

interfacial polarization mechanism.^{35,36} At lower frequencies the space charge accumulation and short-range dipole-dipole interactions at the semiconducting Ni(OH)₂ NBs-insulating PVDF interfaces result in strong interfacial polarization as well as giant dielectric constant. Though with increasing frequency, the MWS interfacial polarization in the NCs is restricted due to the confinement of the charge carriers and molecular movement but a weak frequency dependency has been observed in the NC samples due to strong interfacial interaction via the formation of hydrogen bonds between the F atoms of polymer matrix and the -OH group of the NBs.^{25, 37} The Debye like dipolar relaxations or tangent loss peaks are mainly for large dielectric response. Interesting fact is that with increasing doping concentration of Ni(OH)₂ NBs, the tangent loss peaks are shifted towards higher frequencies.^{35, 36} This shifting in relaxation peaks are attributed to the strong dipolar relaxation effect caused by the Ni(OH)₂ NBs which is bonded to PVDF matrix via hydrogen bond between the F atom of polymer and -OH group in NBs schematically shown in Figure 8.²⁵

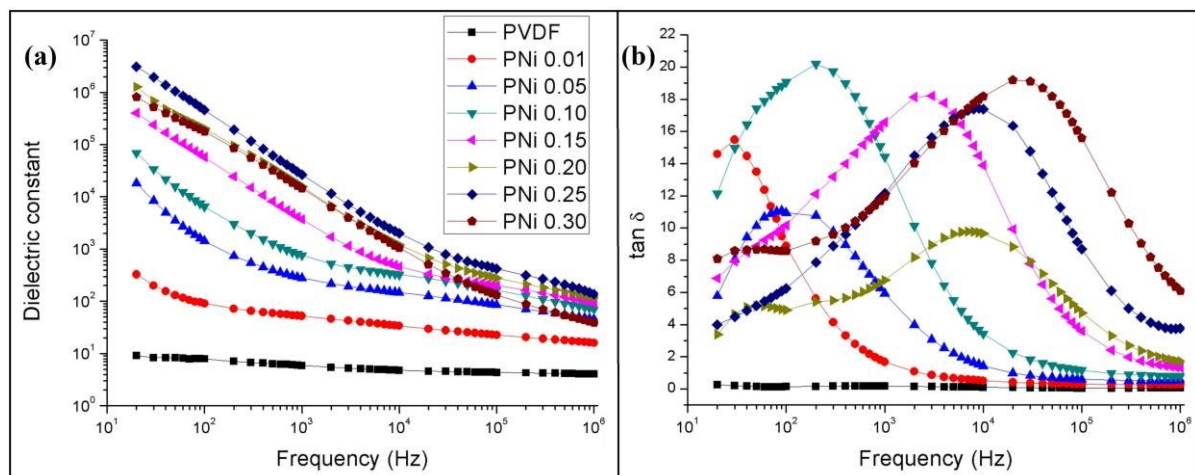


Figure 11: Frequency dependence of dielectric properties of pure PVDF and Ni(OH)₂ NBs modified PVDF thin films: (a) dielectric constant and (b) tangent loss.

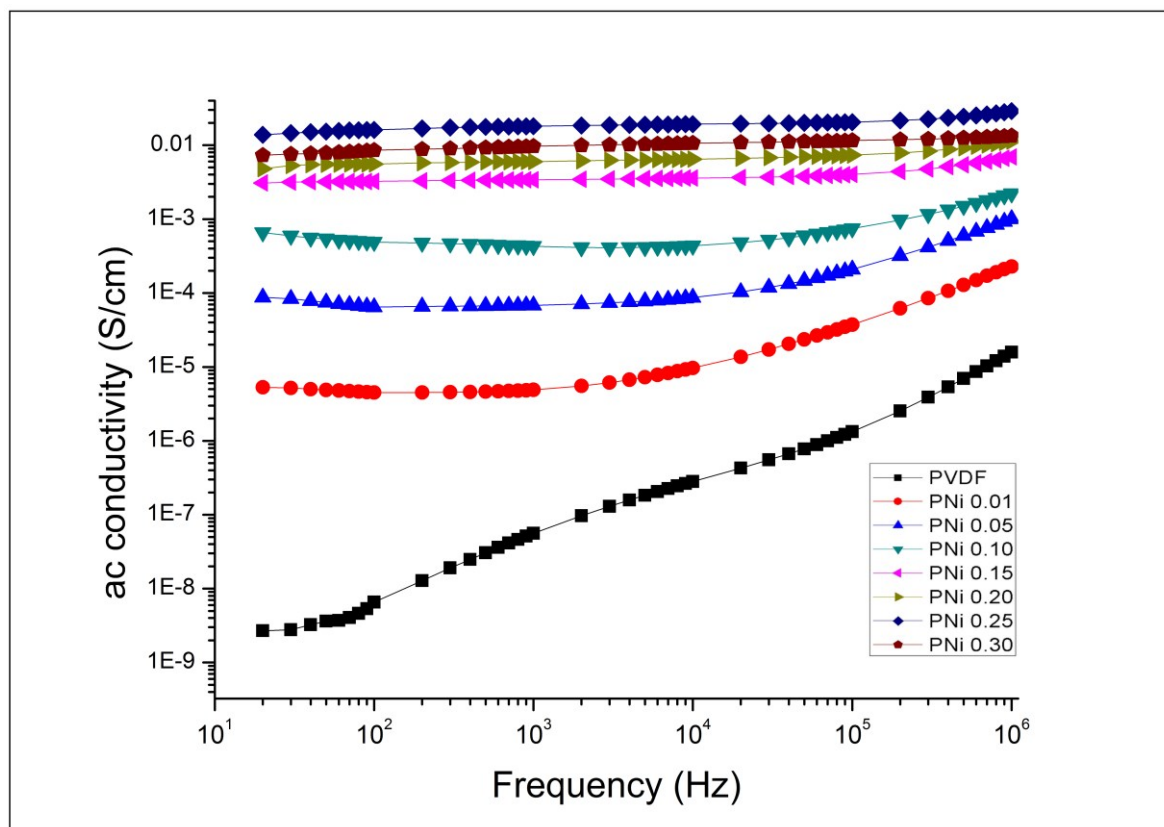


Figure 12: Frequency dependence ac conductivity of pure PVDF and Ni(OH)₂ NBs modified PVDF thin films.

Figure 12 shows the dependence of the ac conductivity of pure PVDF and the Ni(OH)₂ NBs modified PVDF thin films with frequency. The ac conductivity of pure PVDF thin film increases with frequency. But the ac conductivity of Ni(OH)₂ NBs modified PVDF thin films increases slowly than pure PVDF with increasing frequency (PNi 0.01, PNi 0.05 and PNi 0.10) and almost no change in ac conductivity for higher doping of the NBs in PVDF (PNi 0.15, PNi 0.20, PNi 0.25 and PNi 0.30) though the ac conductivity of the samples increases with doping concentration up to 23.1 volume% of NBs. The results suggest that the ac conductivities of the Ni(OH)₂ NBs modified PVDF thin films shows good frequency stability. The conductivity at low frequency region is mainly controlled by dc conductivity and at higher frequencies, it is distinguished by frequency dependent conductivity which confirms the ac conductivity with dipolar polarization effects and dipolar relaxations.⁹ The

molecules of the Ni(OH)₂ NBs modified PVDF thin films are much abstained due to strong hydrogen bond between the F atom of polymer and -OH group in NBs and at high frequency dipolar polarization does not happen due to no availability of time for alignment of the molecules to the applied electric field.^{25, 26} Thus, the Ni(OH)₂ NBs modified PVDF thin films exhibit poor dependence of ac conductivity on frequency. Highest ac conductivity is found for PNi 0.25 about 1.384×10^{-2} S/cm.

4. CONCLUSIONS

Ni(OH)₂ NBs modified PVDF NC thin films have been prepared by a simple soft chemical approach. About 82 % electroactive β phase nucleation is achieved by loading 10.7 volume% Ni(OH)₂ NBs in PVDF matrix. Strong interfacial interaction via hydrogen bonds between the F atoms of the polymer chains and -OH groups of Ni(OH)₂ NBs leads to formation long TTTT conformation on the surfaces of the NBs.

Colossal dielectric constant about 3.1×10^6 at 20 Hz is achieved by loading 23.1 volume% *in situ* Ni(OH)₂ NBs in PVDF matrix and weaker frequency dependency of the ac conductivity is also observed due to the formation of hydrogen bonds in Ni(OH)₂ NBs modified PVDF thin films. So, the highly improved electroactive and dielectric thin films may find use in developing diverse film based energy storage devices, high performance electromechanical devices, piezoelectric nanogenerator, thin film transistors, sensors and actuators.

ACKNOWLEDGEMENTS

Authors are thankful to University Grants Commission (UGC), Government of India (F. 17-76/2008 (SA-1)) for the financial assistance.

REFERENCES:

- 1 A. V. Bune, V. M. Fridkin, S. Ducharme, L. M. Blinov, S. P. Palto, A. V. Sorokin, S. G. Yudin, and A. Zlatkin, *Nature*, 1998, **391**, 874-877.
- 2 S. H. Lim, A. C. Rastogi and S. B. Desu, *J. Appl. Phys.*, 2004, **96**, 5673.
- 3 R. C. G. Naber, C. Tanase, P. W. M. Blom, G. H. Gelinck, A. W. Marsman, F. J. Touwslager, S. Setayesh and D. M. De Leeuw, *Nat. Mater.*, 2005, **4**, 243-248.
- 4 E. Y. Tsybal and H. Kohlstedt, *Science*, 2006, **313**, 181-183.
- 5 H. S. Nalwa, *Ferroelectric Polymers: Chemistry, Physics, and Applications*. Marcel Dekker: New York, 1995.
- 6 T. T. Wang, J. M. Herbert and A. M. Glass, *The Applications of Ferroelectric Polymers*, Chapman and Hall, New York, 1988.
- 7 P. Martins, A. C. Lopes and S. Lanceros-Mendez, *Prog. Polym. Sci.* 2013, **39(4)**, 683-706.
- 8 A. J. Lovinger, *Science* 1983, **220**, 1115-1121.
- 9 P. Thakur, A. Kool, B. Bagchi, S. Das and P. Nandy, *Appl. Clay. Sci.*, 2014, **99**, 149-159.
- 10 D. Shah, P. Maiti, E. Gunn, D. Schmidt, D. D. Jiang and C. A. Batt, *Adv. Mater.*, 2004, **16(14)**, 1173-77.
- 11 T. U. Patro, M. V. Mhalgi, D. V. Khakhar and A. Misra, *Polymer*, 2008, **49(16)**, 3486-3499.
- 12 L. Priya and J. P. Jog, *J. Appl. Polym. Sci.*, 2003, **89(8)**, 2036-2040.
- 13 P. Mishra and P. Kumar, *Compos. Sci. Technol.*, 2013, **88**, 26-32.

- 14 H. P. Xu and Z. M. Dang, *Chem. Phys. Lett.*, 2007, **438(4–6)**, 196–202.
- 15 K. S. Deepa, M. S. Gopika and J. James, *Compos. Sci. Technol.* 2013, **78**, 18-23.
- 16 P. Martins, C. M. Costa, M. Benelmekki, G. Botelho and S. L. Mendez, *Cryst. Eng. Comm.*, 2012, **14(8)**, 2807-2811.
- 17 V. Sencadas, P. Martins, A. Pitães, M. Benelmekki, J. L. G. Ribelles and S. Lanceros-Mendez, *Langmuir*, 2011, **27(11)**, 7241-7249.
- 18 R. Song, G. Xia, X. Xing, L. He, Q. Zhao and Z. Mad, *J. Colloid Interface Sci.*, 2013, **401**, 50-57.
- 19 S. L. Jiang, U. Yu, J. J. Xie, L. P. Wang, Y. K. Zeng and M. Fu, *J. Appl. Polym. Sci.*, 2010, **116(2)**, 838-842.
- 20 J. K. Yuan, S. H. Yao, Z. M. Dang, A. Sylvestre, M. Genestoux, and J. Bai, *J. Phys. Chem. C.*, 2011, **115**, 5515–5521.
- 21 Y. J. Li, M. Xu, J. Q. Feng and Z. M. Dang, *Appl. Phys. Lett.* 2006, **89(7)**, 072902–5.
- 22 W. Wu, X. Huang, S. Li, P. Jiang and T. Toshikatsu, *J. Phys. Chem. C*, 2012, **116(47)**, 24887-24895.
- 23 Y. Zhang, Y. Wang, Y. Deng, M. Li and J. Bai, *ACS Appl. Mater. Interfaces*, 2012, **4(1)**, 65-68.
- 24 P. Thakur, A. Kool, B. Bagchi, S. Das and P. Nandy, *Phys. Chem. Chem. Phys.*, 2015, **17**, 1368-1378.
- 25 T. Zhou, J. W. Zha, R. Y. Cui, B. H. Fan, J. K. Yuan and Z. M. Dang, *ACS. Appl. Mater. Interfaces*, 2011, **3(7)**, 2184-2188.
- 26 B. P. Mandal, K. Vasundhara, E. Abdelhamid, G. Lawes, H. G. Salunke, and A. K. Tyagi, *J. Phys. Chem. C*, 2014, **118**, 20819-20825.

- 27 F. A. Cotton and G. Wilkinson, *Advanced Inorganic Chemistry*, pp 894, *Inter Science*, London 1972.
- 28 Y. Qi, H. Qi, J. Li and C. Lu, *J. Cryst. Growth*, 2008, **310**, 4221-4225.
- 29 J. Yu, S. Wang, B. Cheng, Z. Linb and F. Huang, *Catal. Sci. Technol.*, 2013, **3**, 1782-1789.
- 30 P. Nallasamy and S. Mohan, *Indian J. Pure. Appl. Phys.*, 2005, **43(10)**, 821-827.
- 31 P. Martins, C. M. Costa, J. C. C. Ferreira and S. Lanceros-Mendez, *J. Phys. Chem. B*, 2012, **116(2)**, 794-801.
- 32 Y. Li, X. Huang, Z. Hu, P. Jiang, S. Li and T. Tanaka, *ACS Appl. Mater. Interfaces*, 2011, **3(11)**, 4396-4403.
- 33 T. W. Dakin, *IEEE Elect. Insul. Mag.*, 2006, **22**, 11-28.
- 34 A. Moliton, *Applied Electromagnetism and Materials*. Springer: New York, 2007, Chapter 3.
- 35 C. C. Wang, J. F. Song, H. M. Bao, Q. D. Shen and C. Z. Yang, *Adv. Funct. Mater.*, 2008, **18(8)**, 1299-1306.
- 36 P. Lunkenheimer, V. Bobnar, A. V. Pronin, A. I. Ritus, A. A. Volkov and A. Loidl, *Phys. Rev. B: Condens. Matter Mater. Phys.*, 2002, **66**, 052105.
- 37 P. Thakur, A. Kool, B. Bagchi, N. A. Hoque, S. Das and P. Nandy, *RSC Adv.*, 2015, **5**, 28487-28496.